AIAA 94-0239

Thermocapillary Driven Flow Past Marangoni Instability

V. S. Arpaci and E. Evren-Selamet
Department of Mechanical Engineering
and Applied Mechanics
The University of Michigan,
Ann Arbor, Michigan
A. T. Chai
NASA Lewis Research Center,
Cleveland, Ohio

32nd Aerospace Sciences Meeting & Exhibit
January 10-13, 1994 / Reno, NV

THERMOCAPILLARY DRIVEN FLOW PAST THE MARANGONI INSTABILITY

V. S. Arpaci and **E. Evren-Selamet**
Department of Mechanical Engineering and Applied Mechanics
The University of Michigan, Ann Arbor, Michigan

A. T. Chai
NASA Lewis Research Center, Cleveland, Ohio

Abstract

A fundamental dimensionless number,

$$\Pi_C \sim \frac{Ma}{1+Pr^{-1}},$$

is introduced for thermocapillary driven flows. Here Ma and Pr respectively denote the usual Marangoni and Prandtl numbers. The significance of this number for past Marangoni instabilities is demonstrated in terms of a projection method involving the Godunov discretization for convective terms, as well as the data available in the literature.

1. Introduction

The problem of thermocapillary (surface tension) driven flow continues to attract increased experimental, analytical and computational attention because of its importance to space explorations. Block's (1956) experimental observations supported by Pearson's (1958) analytical study about four decades later than Rayleigh demonstrated that thermocapillary rather than buoyancy is responsible for instability in some of the Benard experiments. For example, drying paints are now known to display steady cellular circulatory flow of the " Benard type " whether the free surface was at the top or bottom of the paint layer. The critical Rayleigh number fails then to predict the flow initiation. Pearson has shown in terms of infinitesimal disturbances that the thermocapillary forces are sufficient to cause this instability characterized by the Marangoni number,

$$Ma = \frac{\Delta\sigma l}{\mu\alpha}, \tag{1}$$

$\Delta\sigma$ being net surface tension, l the thickness of the horizontal liquid layer, μ the dynamic viscosity and α the thermal diffusivity. Note that, by definition,

$$Ma = (\frac{F_C}{F_V})(\frac{Q_H}{Q_K}), \tag{2}$$

F_C and F_V respectively being the thermocapillary tension and viscous forces, Q_H and Q_K the enthalpy flow and conduction. Also, by definition, the Prandtl number is

$$Pr = (\frac{Q_H}{Q_K})(\frac{F_V}{F_I}), \tag{3}$$

F_I being the inertial force. An infinitesimal theory, resting on linearized governing equations, ignores the nonlinear inertial effects and is independent of the Prandtl number. It is then governed by the Marangoni number alone. A nonlinear theory for thermocapillary driven flows past the Marangoni instability depends on the Prandtl number as well as the Marangoni number. A fundamental dimensionless number including the effect of both Ma and Pr so far appears to be overlooked in the literature. The objective of the present study is to introduce this dimensionless number and to discuss the thermocapillary driven nonlinear flows in terms of this number. The study consists of four sections. Following this introduction, Section 2 is devoted to some dimensional considerations, Section 3 to a computational integration, and Section 4 to a discussion of results and some conclusions.

2. Dimensional Consideration

For reasons to be clear later, consider first a flow driven by buoyant as well as thermocapillary forces,

$$F_B + F_C \sim F_I + F_V, \tag{4}$$

F_B being the buoyant force. The thermal energy balance for this flow is

$$Q_H \sim Q_K. \tag{5}$$

Now, rearrange Eq. (4) as

$$\frac{F_B + F_C}{F_I + F_V} \sim \frac{F_B/F_V + F_C/F_V}{1 + F_I/F_V} \tag{6}$$

and Eq. (5) as

$$Q_H/Q_K. \tag{7}$$

Note that the numeral 1 in the denominator of Eq. (1) implies an order of magnitude. Explicitly,

$$F_B \sim g\Delta\rho l^3, \qquad F_V \sim \mu V l,$$

$$F_C \sim \Delta\sigma l, \qquad F_I \sim \rho V^2 l^2$$

$$Q_H \sim \rho c_p V T l^2, \qquad Q_K \sim k T l,$$

and

$$\frac{F_B}{F_V} \sim \frac{g\Delta\rho l^2}{\mu V}, \quad \frac{F_C}{F_V} \sim \frac{\Delta\sigma}{\mu V}, \quad \frac{F_I}{F_V} \sim \frac{\rho V l}{\mu}, \tag{8}$$

$$\frac{Q_H}{Q_K} \sim \frac{\rho V l}{k}, \tag{9}$$

where ρ is the density, c_p the specific heat at constant pressure, V the velocity, T the temperature, l a characteristic length and Δ is the difference in surface tension or density.

Equation (6) yields, in terms of Eq. (8) ,

$$\frac{g\Delta\rho l^2/\mu V + \Delta\sigma/\mu V}{1 + \rho V l/\mu}, \tag{10}$$

and Eq. (7) gives, in terms of Eq. (9) ,

$$\rho c_p V l/k. \tag{11}$$

For thermocapillary and/or buoyancy driven flow(s), V is a dependent variable. Consequently, neither Eq. (10) nor Eq. (11) is an ultimate dimensionless number for these flows. The elimination of V between Eq. (10) and Eq. (11) leads to this number,

$$\frac{(F_B/F_V + F_C/F_V)Q_H/Q_K}{(1 + F_I/F_V)Q_K/Q_H},$$

or, explicitly,

$$\Pi_{BC} \sim \frac{(g/\nu\alpha)(\Delta\rho/\rho)l^3 + \Delta\sigma l/\mu\alpha}{1 + \alpha/\nu}, \tag{12}$$

or,

$$\Pi_{BC} \sim \frac{Ra + Ma}{1 + Pr^{-1}}. \tag{13}$$

Note that the numeral 1 in the denominator of Eqs. (6), (10), (12) and (13) implies an order of magnitude. The two limits of Eq. (13), respectively corresponding to the buoyancy driven and surface tension driven flows, are

$$\lim_{\Delta\sigma \to 0} \Pi_{BC} \to \Pi_B \sim \frac{Ra}{1 + Pr^{-1}}, \tag{14}$$

$$\lim_{g\Delta\rho \to 0} \Pi_{BC} \to \Pi_C \sim \frac{Ma}{1 + Pr^{-1}}. \tag{15}$$

Although there is abundant analytical and experimental evidence in the literature, Π_{BC} and its limits (Π_B, Π_C) surprisingly remain overlooked. Only, the following limits for $F_I \to 0$ $(Pr \to \infty)$,

$$\lim_{F_I \to 0} \Pi_B \to Ra \tag{16}$$

and

$$\lim_{F_I \to 0} \Pi_C \to Ma \tag{17}$$

are well known. Some of the literature is cited below for support of the respective relevance of Π_B and Π_C given by Eqs. (14) and (15) for buoyancy and thermocapillary driven flows.

An approximate analysis by Squire (1938) of buoyancy driven laminar flow next to a vertical wall yields for heat transfer

$$Nu = 0.508 Pr^{1/2}(Pr + \frac{20}{21})^{-1/4}[\frac{gh^3(T_1 - T_0)}{\nu^2 T_0}]^{1/4}$$

which can be rearranged as

$$Nu = 0.508\Pi_B^{1/4}, \tag{18}$$

where Nu is the Nusselt number, and

$$\Pi_B = \frac{Ra}{0.952 + Pr^{-1}}. \tag{19}$$

An experimental study by Krishnamurti (1973) shows the cascade of transitions in buoyancy driven flows past the Benard instability (Fig. 1). Among these transitions, for example, the second transition can be qualitatively related to the first transition by the simple model,

$$(Ra_c)_{II} = (Ra_c)_I + \frac{(\Delta Ra_c)_I^{II}}{1 + Pr^{-1}},$$

or

$$(Ra_c)_{II} = (Ra_c)_I + (\Delta\Pi_B)_I^{II},$$

where

$$(\Delta\Pi_B)_I^{II} = \frac{(\Delta Ra_c)_I^{II}}{1 + Pr^{-1}}, \tag{20}$$

and

$$(\Delta Ra_c)_I^{II} = (Ra_c)_{II} - (Ra_c)_I, Pr \to \infty.$$

For liquid metals, $Pr \ll 1$ and Eq. (20) is reduced to

$$(\Delta\Pi_B)_I^{II} \to (\Delta Ra_c)_I^{II} Pr \tag{21}$$

which is the tangent of Eq. (20) between domains I and II shown in Fig. 2. As $Pr \to 0$, all transitions collapse on the first transition which now directly leads to turbulence (Domain I in Fig. 2). For gases, $Pr \sim 1$ Eq.(20) applies as is. However, because Pr of gases varies very little, Eq.(20) covers now a narrow band in the middle of Domain II of Fig. 2 (g-band). For water, $6 < Pr < 30$, Eq.(20) continues to apply with a reduced inertial effect (but because Pr of water varies more than that of gases) over a wider range than that of gases (w-band). For viscous oils, $10^2 < Pr < \infty$, and Eq.(20) is reduced to

$$(\Delta\Pi_B)_I^{II} \to (\Delta Ra_c)_I^{II} \tag{22}$$

which is independent of Pr because of the negligible inertial effect (Domain III in Fig. 2).

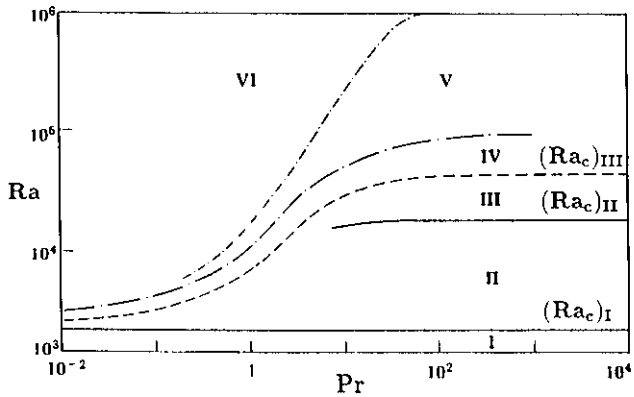

Fig. 1 Cascade of flow regimes : I-No motion; II-steady 2-D motion; III-steady 3-D motion; IV-V-unsteady 3-D motion (from periodic to chaotic); VI-turbulent motion (Krishnamurti 1973).

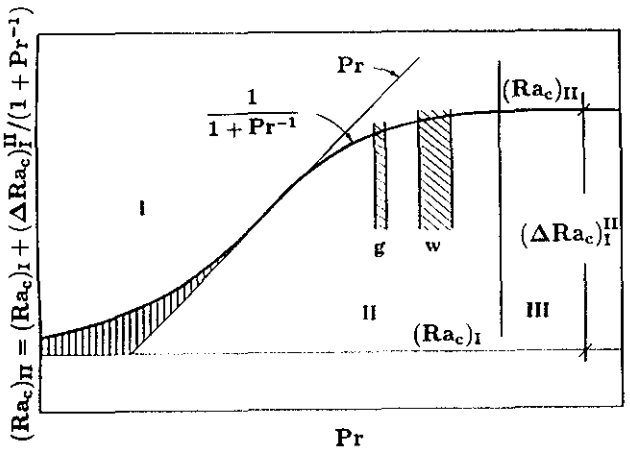

Fig. 2 Second transition versus Prandtl number: g-band for gases, w-band for water.

Beginning with Malkus and Veronis (1958) for free boundaries, and continuing with Schluter, Lortz and Busse (1965), Gough, Spiegel and Toomre (1975) and Busse (1985) for rigid boundaries, a first order inertial effect is incorporated into heat transfer by an expansion in powers of Pr^{-1},

$$\frac{Nu-1}{Ra-Ra_c} = (C_1 + C_2 Pr^{-1} + C_3 Pr^{-2} + ..) \qquad (23)$$

which can be rearranged in view of

$$(1 - Pr^{-1} + Pr^{-2} - Pr^{-3} + ..) \equiv 1 + Pr^{-1})^{-1}.$$

as

$$\frac{Nu-1}{\Delta Ra_c} \sim (1+Pr^{-1})^{-1}, \qquad (24)$$

or,

$$Nu - 1 \sim \Delta \Pi_B, \qquad (25)$$

In recent studies, Arpaci (1986, 1990) introduces the microscales for buoyancy driven turbulent flows, and in terms of these scales, proposes a heat transfer model based on Π_B

$$Nu \sim \frac{\Pi_B^{1/3}}{1-\Pi_B^{-1/9}}, \quad \Pi_B \sim \frac{Ra}{1+Pr^{-1}} \qquad (26)$$

which correlates the entire experimental data of the literature on the turbulent flow originating from the Benard problem.

There is no reference to Π_C in the literature on thermocapillary driven instabilities. Clearly an infinitesimal amplitude theory, being independent of inertial forces, neglects the effect of Pr number. In this case, as is mentioned earlier (recall Eq.17), Π_C is reduced to Ma. However, a finite amplitude or nonlinear theory depends on Pr and, consequently , on Π_C. Nonlinear theories for laterally unbounded layer based on leading-order bifurcation methods appear to be exhausted by Cloot and Lebon (1984). For laterally bounded layer, Rosenblat al. (1982 a,b) investigate the problem with slippery sidewalls. In these elaborate mathematical studies, the physical significance of Π_C on flow past the first transition appears to remain unnoticed. Cloot and Lebon consider only the range of Pr> 1 (by the specific values of Pr=7, 70, 500) for which the inertial effect is negligible, and $\Pi_C \rightarrow$ Ma. This effect becomes significant as Pr $\rightarrow$ 0, and the range Pr $\lesssim$ 1 is essential for the recognition of Π_C. Rosenblat *et al.* (1982a) consider the specific values of Pr=0.1, 1, 10, ∞ which are utilized here to demonstrate a trendwise dependence on Π_C (Arpaci 1990 illustrates the need of extensive data for accurate dependence on Π_B).

An extension of the literature on buoyancy to thermocapillary, readily yields for heat transfer

$$Nu - 1 \sim A^2, \qquad (27)$$

A being the Landau amplitude of thermocapillary fluctuations, or, in terms of Eq.(25),

$$Nu - 1 \sim \Delta \Pi_C. \qquad (28)$$

Noting Eq.(15),

$$Nu - 1 \sim \frac{Ma - Ma_c}{1 + Pr^{-1}}, \qquad (29)$$

or,

$$\frac{Nu-1}{Ma-Ma_c} = \frac{C_0}{1+C_1 Pr^{-1}}, \qquad (30)$$

C_0 and C_1 being numerical constants. For the Landau amplitude, Rosenblat *et al.* (1982a) gives

$$A^2 \sim \frac{1}{\omega}(Ma - Ma_c) \qquad (31)$$

by which Eq.(27) becomes

$$\frac{Nu-1}{Ma-Ma_c} = \frac{C}{\omega}, \qquad (32)$$

again, C being a numerical constant depending only on the aspect ratio. Table 1, rearranged from Table 1 and 2 of Rosenblat *et al.*, gives ω for two aspect ratio a=0.9, 1.5.

a	Pr	0.1	1	10	∞
0.9	ω x 10^{-2}	12	1.6	1.1	1.
1.5		6.2	0.98	0.5	0.45

Table 1

Fig. 3 shows $(Nu-1)/(Ma-Ma_c)$ against Pr for C = 10^2, assumed for graphical convenience. There is no information on C in Rosenblat *et al.* However, an assumed C affects the graphical scale but not the Prandtl dependence.

The rest of the present study carries out a modest computational work beyond a first-order bifurcation discussed in Rosenblat *et al.* (1982a,b) analytical studies. The objective is the numerical recognition of Π_C beyond the analytical bounds. In the selection of this numerical method, special attention is paid to accurate computation of inertial effects which are responsible for the Prandtl number effect. To keep the computational work from being exhaustive, the flow is assumed to be two-dimensional in a laterally bound horizontal layer. The side walls are adiabatic, and all boundaries are non-slippery except for the free top surface. The liquid is cooled at the free upper surface by heat transfer to ambient.

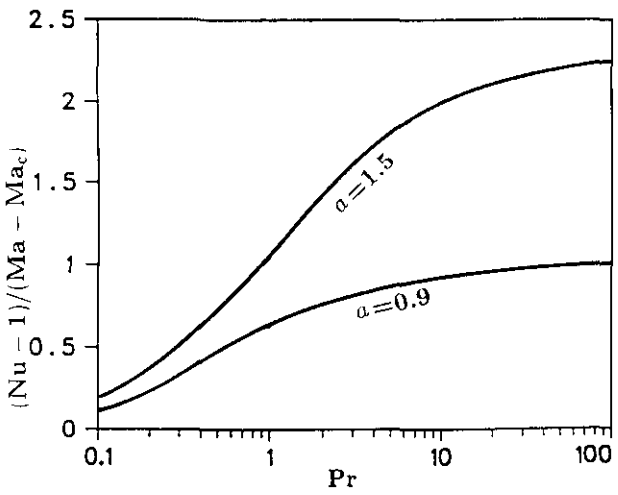

Fig. 3: (Nu − 1)/(Ma − Ma$_c$) versus Pr for two aspect ratios.

3. Numerical Method

The main features of the computational procedure described by Evren-Selamet *et al.* (1991,1992) are summarized here for later convenience. The projection method involving a Godunov-type discretization for inertial terms is utilized. The method involves two steps based on a decomposition of the momentum equations. The first step computes an auxiliary velocity field $\hat{U}$,

$$\frac{\hat{U}-U^n}{\Delta t} = -\Theta[(U.\nabla)U]^{n+1} - (1-\Theta)[(U.\nabla)U]^n + Pr[\Theta\nabla^2\hat{U} + (1-\Theta)\nabla^2 U^n] \quad (33)$$

which is the momentum equation without pressure gradient. Here $U = u\mathbf{i} + v\mathbf{j}$ and Θ is a weighting factor between 0 and 1. The discretization of the Laplacian of the diffusion terms is done by a standard finite difference approximation. In the solution of Eq. (33), the convective term is calculated by a Godunov discretization including the solution of a Riemann problem as defined by Bell and Glaz (1987). In the second step, $\hat{U}$ obtained from Eq. (33) is corrected for a divergence-free velocity field including the effect of pressure gradient. The spatial discretization is based on the staggered grid system. An advantage of using the staggered mesh is that the boundary conditions only for temperature and velocity components are needed, while those for pressure are not. The bottom boundary condition on temperature is

$$\theta = 1 \text{ at } y = 0.$$

The top boundary condition, in dimensionless form, is

$$\frac{\partial\theta}{\partial t} = \frac{\partial^2\theta}{\partial x^2} + (\frac{\partial\theta}{\partial y} - \mathrm{Bi}\theta)\frac{2}{\Delta y}. \quad (34)$$

where Δy is the grid size in y direction, Bi=hH/k the Biot number ; k thermal conductivity of the fluid and h heat transfer coefficient on upper surface. The side walls are insulated,

$$\frac{\partial\theta}{\partial x} = 0 \text{ at } x = 0 \text{ and } x = a \quad (35)$$

where a is the aspect ratio (length/height). On rigid walls both components of velocity are taken to be zero. For free top surface only the normal component is taken to be zero. The condition for horizontal component by considering the shear stress in this direction is

$$\mu\frac{\partial u^*}{\partial y^*} = \frac{\partial\sigma}{\partial T}\frac{\partial T}{\partial x^*} \quad \text{at} \quad y^* = H \quad (36)$$

or, in dimensionless form (see Dijkstra and van de Vooren 1989)

$$\frac{\partial u}{\partial y} = \mathrm{Ma}^*\frac{\partial\theta}{\partial x}, \quad (37)$$

where

$$\mathrm{Ma}^* = \mathrm{Ma}\frac{1+\mathrm{Bi}}{\mathrm{Bi}}$$

and Ma is the Marangoni number defined by Eq. (1). The upper surface of the liquid is assumed to have large-enough surface tension which allows the surface deformation be neglected.

4. Results and Discussion

A fundamental dimensionless number,

$$\Pi_C \sim \frac{Ma}{1+Pr^{-1}},$$

is introduced for thermocapillary driven flows. Here Ma and Pr respectively denote the usual Marangoni and Prandtl numbers. The significance of this number for past Marangoni instabilities is demonstrated in terms of the analytical studies available in the literature.

Further support for Π_C is provided by a modest computational program which is carried out on two-dimensional (29x29,and 29x59) regular meshes for two aspect ratios (a=1 and 2). Figure 4 shows the velocity and temperature fields for Pr=7 and Bi=10 for two Marangoni numbers. For Ma =800, one roll rotating counter-clockwise appear with its center close to top. Isotherms are distorted accordingly due to convection heat transfer. Toward the lower part of the container, the isotherms tend to become parallel to the bottom wall, as expected. The result for Ma=1500 is similar to what Jackson and Winters (1984) obtained for Ra=10^4 for the Rayleigh-Benard problem. They found two cell (like ours) or one cell depending on the initial conditions. In the present case, one main roll appear in the early stage then a corner roll initiates and begins to grow, it reduces the size of the main roll, and eventually becomes identical in size to but rotating in the opposite direction of the main roll. The fluid rises at the middle and sinks along the container walls. The temperature field is again distorted mostly in upper part of container due to convection heat transfer.

When the aspect ratio is increased to 2, two rolls appear at the steady state for Ma=800 and 1500. The stationary state is symmetric with respect to the vertical centerline. The velocity vectors and isotherms for the values of Ma=800 and 1500, which are resembling buoyancy driven convection, are shown in Fig. 5. The effect of the velocity pointing upward of the centerline is increased with increasing Ma as

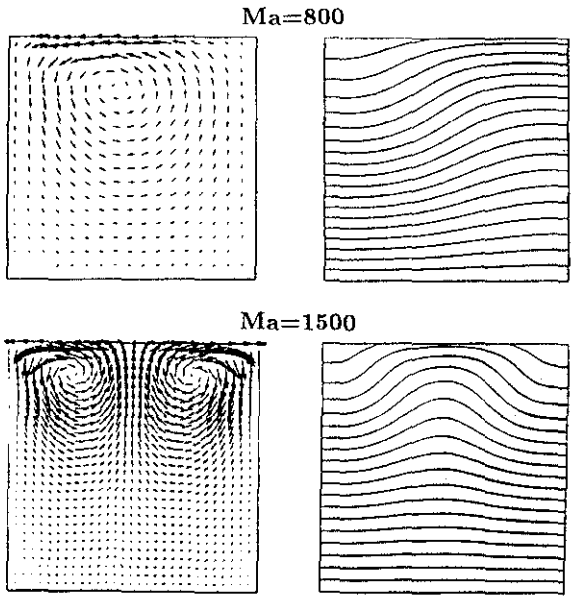

Fig. 4: The velocity vectors with the length scales of 0.01 and temperature contours with the increments of 0.05 for a=1, Bi=10, and Pr=7.

clearly seen in the temperature contour plot.

Pearson gives Ma_c =413.5 at Bi=10 for infinite layer of fluid. We obtained pure conduction solution at this critical value of Ma for a=2. Clearly the critical Marangoni number for the onset of surface-tension-driven convection should be higher for bounded layers. The average Nusselt number which accounts for the heat transfer through the enclosure, $\overline{Nu}$, is determined by the numerical integration over the bottom wall. The history of $\overline{Nu}$ reveals that $\overline{Nu}$ is large at the beginning of the process because of high temperature gradients near the wall then it decreases with time and converges to the steady state.

Numerically obtained $(Nu-Nu_c)/(Ma-Ma_c)$ is plotted against Pr in Fig. 6 for a = 2 and Bi=10. The simultaneous inspection of Figs. 1, 2, 3 and 6 clearly demonstrate the significance of Π_{BC} and the identical intrinsic dependency of buoyancy and thermocapillary driven flows on the Prandtl number.

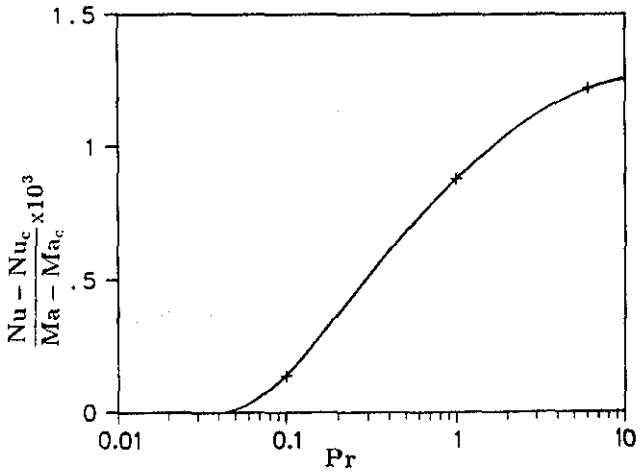

Fig. 6: Variation of $(Nu - Nu_c)/(Ma - Ma_c)$ with Pr for a=2 and Bi=10.

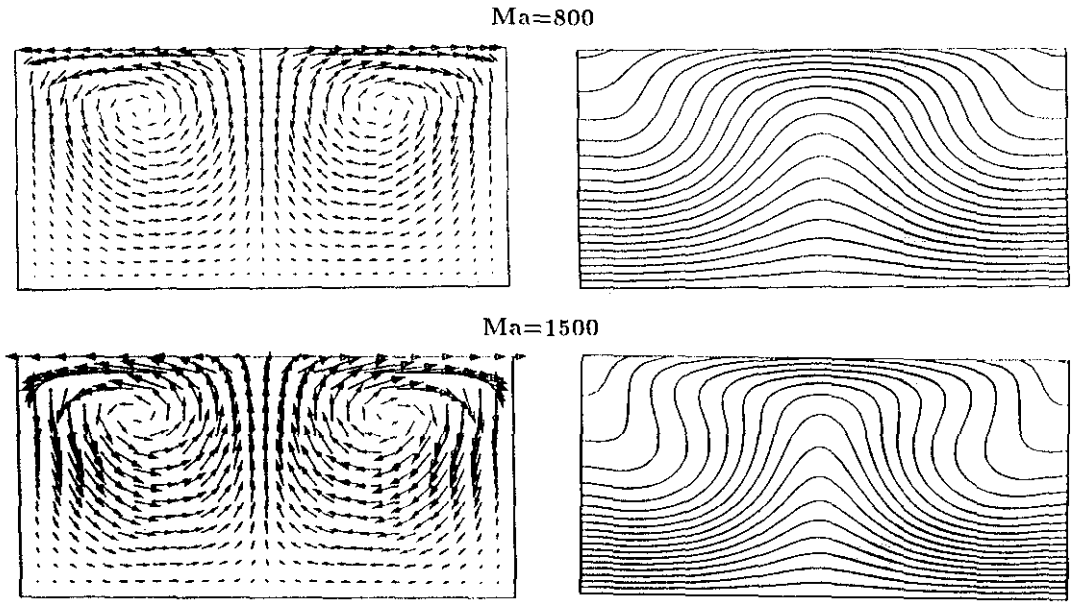

Fig. 5: The velocity vectors with the length scales of 0.01 and temperature contours with the increments of 0.05 for a=2, Bi=10 and Pr=7.

References

[1] **Arpaci, V.S.** 1986, Microscales of Turbulence and Heat Transfer Correlations, *Int. J. Heat Mass Transfer* **29**, 1071.

[2] **Arpaci, V.S.** 1990, Microscales of Turbulence and Heat q Transfer Correlations, *Annual Review of Heat Transfer*, **3**, 195,(Edited by C. L. Tien), Hemisphere Publishing Corporation.

[3] **Bell, J. B. Glaz, H. M.** 1987, A second order projection method for viscous, incompressible flow, *AIAA 8th Computational Fluid Dynamics Conf.* Honolulu, Hawaii.

[4] **Busse, F. H.** 1985, Transition to turbulence in Rayleigh-Benard convection. In *Hydrodynamic Instabilities and the transition to turbulence*, second edition, eds. H. L. Swinney and J. P. Gollub, pp.97-137, Springer-Verlag, Berlin.

[5] **Block, M. J.** 1956, Surface tension as the cause of Benard cells and surface deformation in a liquid film, *Nature* **178**, 650.

[6] **Cloot, A. Lebon, G.** 1984, A nonlinear stability analysis of the Benard-Marangoni problem, *J. Fluid Mech.* **145**, 447.

[7] **Dijkstra, H. A. van de Vooren, A. I.** 1989, Multiplicity and stability of steady solutions for Marangoni convection in a two-dimensional rectangular container with rigid sidewalls, *Numerical Heat Transfer*, Part A **16**, 59.

[8] **Evren-Selamet, E.** 1991, Simulation of Laminar Buoyancy-Driven Flows in an Enclosure, PhD. Thesis, University of Michigan, Ann Arbor, MI.

[9] **Evren-Selamet, E., Arpaci, V. S. Borgnakke, C.** 1992, Simulation of Laminar Buoyancy-Driven Flows in an Enclosure, *Numerical Heat Transfer*, Part A **22**, 401.

[10] **Gough, D. 0., Spiegel, E. A., Toomre, J.** 1975, Modal equations for cellular convection, J. Fluid Mech. **68**, 695.

[11] **Jackson, C. P. Winters, K. H.** 1984, A Finite-Element Study of the Benard Problem Using Parameter-Stepping and Bifurcation Search, *International Journal for Numerical Methods in Fluids*, **4**, 127

[12] **Krishnamurti, R.** 1973, Some further studies on the transition to turbulent convection, *J. Fluid Mech.* **60**, 285.

[13] **Malkus, W. Veronis, G.** 1958, Finite amplitude cellular convection, *J. Fluid Mech.* **4**, 225

[14] **Pearson J. R. A.** 1958, On convection cells induced by surface tension, *J. Fluid Mech.* **4**, 489.

[15] **Rosenblat, S., Davis, S. H. Homsy, G. M.** 1982a, Nonlinear Marangoni convection in bounded layers. Part 1. Circular cylindrical containers, *J. Fluid Mech.* **120**, 91.

[16] **Rosenblat, S., Davis, S. H. Homsy, G. M.** 1982b, Nonlinear Marangoni convection in bounded layers. Part 2. Rectangular cylindrical containers, *J. Fluid Mech.* **120**, 123.

[17] **Schluter, A. Lortz, D. Busse, F.** 1965, On the stability of steady finite amplitude convection, *J. Fluid Mech.* **23**, 129.

[18] **Squire, H. B.** 1938, Free convection from a heated vertical plate, Modern developments in fluid mechanics (ed. Goldstein), Oxford, Vol.2, 638.